

Sulfur-doped Graphene-coated Graphite Foil as Disposable Electrodes for Electrochemical Sensing

Manxia Dai, Shuang Ding, Wei Shi, and Lijun Bian*

Department of Chemistry, Northeastern University, Shenyang 110819, China

*E-mail: bianlijun@mail.neu.edu.cn,

Received: 7 June 2022 / Accepted: 31 July 2022 / Published: 10 September 2022

In this study, sulfur-doped graphene-coated graphite foil (SGGF) was obtained using an in-situ cathodic exfoliation method. Graphene modified on the surface of graphite improves its specific surface area. Cathodic exfoliation prevents the formation of oxygen-containing groups, resulting in high conductivity. The S-doping also improved the charge-carrier concentration and conductivity of the SGGF. The high surface area and conductivity make SGGF a promising electrode for simultaneously detecting ascorbic acid, dopamine, and uric acid. The current responses of the SGGF electrodes were linear with their concentration. The linear concentration ranges were 1 – 4 mM, 1 – 25 μ M, and 1 – 25 μ M with detection limits of 47, 0.12, and 0.15 μ M, respectively.

Keywords: disposable electrode; electrochemical sensing; S-doped graphene

1. INTRODUCTION

Ascorbic acid (AA), dopamine (DA), and uric acid (UA) are important biomolecules that coexist in the extracellular fluid and serum. The detection and quantification of these biomarkers are crucial in diagnosing, preventing, and treating diseases such as schizophrenia, Parkinson's, and gout[1, 2]. The low cost and high sensitivity of electrochemical detection have made it a popular method for detection of the biomarkers [3]. Conventional electrodes exhibit overlapping voltammetric responses to AA, DA, and UA because of their similar oxidation potential. Therefore, several types of materials, such as polymers[4, 5], metal oxides[6, 7], and carbon-based materials[8, 9], have been used to modify traditional electrodes to produce well-separated peaks and improve their performance.

Graphene, single-layer graphite with a two-dimensional honeycomb structure, has been widely applied in batteries[10], capacitors[11, 12], and electrochemical sensors[8]. Electrochemical exfoliation has been extensively used to prepare graphene because of its simplicity, low cost, and high efficiency[13, 14]. In terms of exfoliation mechanism, there are two types of electrochemical exfoliation, anodic and

cathodic exfoliation. Anodic exfoliation has been conducted in various types of electrolytes, including ionic liquids[15, 16], H₂SO₄, H₃PO₄[17, 18], ((NH₄)₂SO₄, Na₂SO₄, and K₂SO₄[19, 20]. Oxygen-containing groups were introduced during the anodic exfoliation process and defects were generated on the edges of graphene sheets. Consequently, graphene was structurally damaged[21]. Cathodic exfoliation was usually performed in organic solutions containing cations such as Li⁺ and TBA⁺ [22, 23]. Graphene obtained through cathodic exfoliation exhibited higher electrical conductivity, lower structural defects, and oxygen-containing groups compared with graphene obtained through anodic exfoliation [24]. However, the exfoliation efficiency of cathodic exfoliation is low, it is time-consuming and usually requires the incorporation of the sonication step. In addition, organic solvents sensitive to water and oxygen are used for the cathodic exfoliation, impeding their practical applications[18]. Graphene obtained through the electrochemical exfoliation process needs to be filtered, purified, dried, and immobilized before it can be used in electrochemical sensors, electrochemical energy storage, and other applications. Therefore, developing a simple, low-cost approach to synthesize graphene is still challenging.

In this study, graphite foil (GF) was modified with partially exfoliated graphene through cathodic exfoliation in a common inorganic solution containing Na₂SO₄ and Na₂S₂O₃. The doped sulfur was simultaneously introduced into the graphene sheets during the exfoliation process. Changes in the surface morphology of the GF after modification were observed using scanning electron microscopy (SEM). The chemical structure of the sulfur-doped graphene-coated graphite foil (SGGF) was characterized through Raman spectroscopy and X-ray photoelectron spectroscopy (XPS). SGGF were used as disposable electrodes for detecting AA, DA, and UA to eliminate the fouling caused by the accumulation of oxidation products on the surface of electrodes. The SGGF electrodes exhibited high selectivity for the detection of AA, DA, and UA, and they could be detected individually or simultaneously.

2. EXPERIMENTAL

2.1. Preparation of SGGF electrodes

The SGGF electrode was obtained through potentiostatic treatment in a mixed solution containing 0.5 M Na₂S₂O₃ and Na₂SO₄ at potentials of -1.5, -1.6, -1.7 V. The obtained samples were designated as SGGF1, SGGF2, and SGGF3. Before the electrochemical test, the SGGF electrodes were thoroughly washed with water.

2.2. Characterization

To compare the variation in GF before and after modification, GF and SGGF were characterized through XPS (ESCALAB 250Xi, Thermo Scientific Escalab, USA), Raman spectroscopy (Thermo Fisher DXR2xi, USA), and SEM (Hitachi SU-8010, Japan).

3. RESULTS AND DISCUSSION

3.1 Characterization of SGGF

The modification of GF with S-doped graphene was realized through cathodic exfoliation using 0.5 M $\text{Na}_2\text{S}_2\text{O}_3$ and Na_2SO_4 as the exfoliation agent and dopant, respectively. GF was treated electrochemically at potentials of -1.5 , -1.6 , and -1.7 V for 25 min. The morphologies of the SGGF and GF electrodes were investigated and the surface of GF was compact and flat (Figure 1a). After electrochemical exfoliation at -1.5 V, the surface morphology of SGGF1 did not change (Figure 1b). The potential of -1.5 V was not sufficient to force enough ions to intercalate into the graphite sheets to partially exfoliate graphene. When the potential of the electrochemical treatment decreased to -1.6 V, there was sufficient driving force to insert more ions into graphite and expand it. Therefore, multilayer graphene sheets were observed (Figure 1c). More ions intercalated into graphite, and gases such as H_2 and SO_2 were generated on the surface of graphite at -1.7 V, which facilitated the exfoliation of graphene. Consequently, the surface of SGGF3 was covered with graphene nanosheets (Figure 1d). The graphene sheets were separated from each other and there were several wrinkles on their surface, resulting in the highest specific surface area of SGGF3. A high specific surface area provides a larger contact area between the electrode and electrolyte, and more active centers, enhancing electrocatalytic performance.

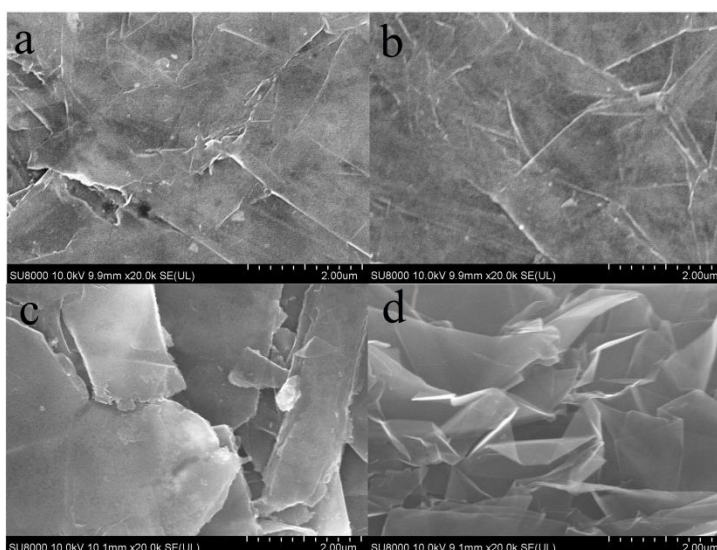


Figure 1. SEM images of (a) GF, (b) SGGF1, (c) SGGF2, and (d) SGGF3.

The Raman spectra of GF and SGGF3 are illustrated in Figure 2. There are two main peaks observed at ~ 1590 and 2700 cm^{-1} in the GF spectrum, which are attributed to the G and 2D bands, respectively [25, 26]. After electrochemical modification with graphene, a new peak attributed to the D band was observed in the SGGF3 spectrum. The D band is associated with topological defects, including structural distortions and vacancies in the graphene lattice caused by S-doping [27, 28]. An appropriate

number of defects in graphene is vital for its electrochemical properties because electrochemical reactions occur preferentially in defects [29, 30]. The ratio of the D to G band (I_D/I_G) was 0.15, which is significantly less than that of the graphene obtained through anodic exfoliation [31, 32]. Cathodic exfoliation can prevent the oxidation of graphene; therefore, it was more conducive for maintaining the inherent sp^2 C=C bond.

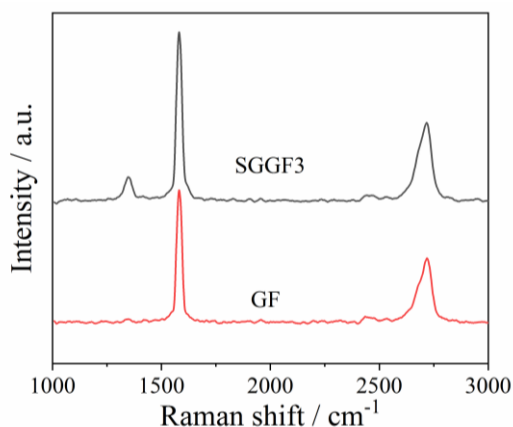


Figure 2. Raman spectra of GF and SGGF3.

To confirm the successful doping of graphene with S, the SGGF3 atoms and their states were analyzed through XPS. The content of O in SGGF3 was approximately 3.6 at%, which is significantly less than that of the graphene obtained through anodic exfoliation [24, 33, 34]. This further proves that cathodic exfoliation prevents the formation of oxygen-containing functional groups. The C 1s high-resolution spectra are illustrated in Figure 3a. The peaks observed at 284.7, 285.3, 287.5, and 290.5 eV are attributed to C=C, C-S/C-O, O-C=O, $\pi=\pi^*$, respectively [20, 35, 36]. The appearance of the $\pi=\pi^*$ shake-up signal indicates that SGGF3 exhibits high electrical conductivity [37]. The binding energies observed at 163.9 and 165.2 eV in the S 2p spectrum (Figure 3b) are attributed to the -C-S-C- structure, which exhibits higher electrochemical activity than other sulfur-containing groups [29]. The peak observed at 170.5 eV indicates that the functional groups -C-SO_x-C- ($x = 2, 3$) exist on the surface of graphene [38, 39].

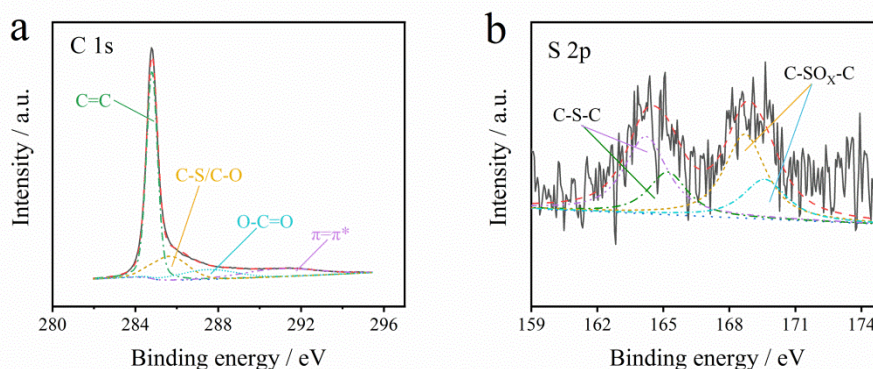


Figure 3. High-resolution C 1s spectrum (a) and S 2p spectrum (b).

3.3 Electrochemical behavior of the SGGF3 electrode

CV tests were conducted in a 5 mM $\text{Fe}(\text{CN})_6^{3-/4-}$ solution to investigate the electroactivity of the SGGF3 electrode. As shown in Figure 4a, the peak potential separation of $\text{Fe}(\text{CN})_6^{3-/4-}$ decreased and the redox peak current increased at the SGGF3 electrode. The results indicated that SGGF3 exhibits a higher electron transfer rate and has a larger electroactive surface area [40, 41]. The electrochemically active areas of the GF and SGGF3 were 0.37, and 2.4 cm^2 , respectively, which were determined using the Randles–Ševčík equation [42]. These results are consistent with the SEM results.

Figure 4b illustrates the Nyquist plots of the GF and SGGF3 electrode, including a semicircle in the high-frequency region and a straight line in the low-frequency region. The smaller semi-circular diameter of the SGGF3 indicates a lower charge-transfer resistance. This is attributed to the high conductivity of the graphene obtained through cathodic exfoliation, which prevents the formation of oxygen-containing functional groups. As electron donors, S atoms have been demonstrated in previous studies to improve the conductivity and charge-carrier concentration of the carbon matrix [28]. The high electrical conductivity makes the SGGF3 electrode a promising electrochemical sensor [43].

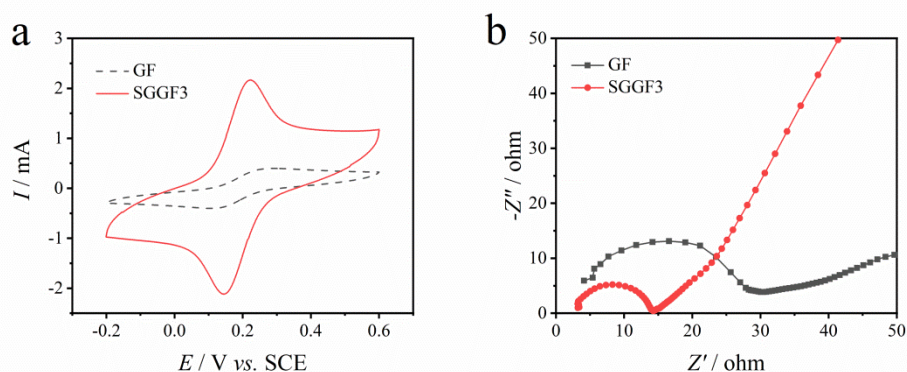


Figure 4. (a). CVs and (b) Nyquist plots of the GF and SGGF3 in the solution of 5 mM $\text{Fe}(\text{CN})_6^{3-/4-}$ with 0.1 M KCl as the supporting electrolyte.

3.3 Electrochemical response of AA, DA, and UA on SGGF3 electrodes

The electrochemical oxidation of AA, DA, and UA at the SGGF3 and GF electrodes was compared through CV, as shown in Figure 5a-c. They exhibited similar responses at the two electrodes and their oxidation peak potentials at GF and SGGF3 were almost the same. However, the oxidation peak currents at SGGF3 electrodes are significantly higher than those at the GF electrodes. The large specific surface of SGGF3 provides more active sites for oxidation, thus, the currents on SGGF3 are significantly higher.

A CV test was also performed in a solution containing the three species, as shown in Figure 5d. The oxidation peaks in the CV curve of GF were not clear, indicating poor sensitivity. Conversely, the oxidation peaks on the curve of SGGF3 can be observed clearly at ~ -0.1 , 0.2, and 0.3 V; the three peaks are separate from each other. This makes it possible to detect the three species individually and simultaneously. SGGF3 exhibited a significantly higher current response than GF, demonstrating its

superior electrocatalytic activity. Graphene with a high surface area on SGGF3 provides more active sites for electrocatalysis, and S-doping accelerates the transfers of electrons to biomolecules in the electrochemical reactions, leading to improved electrocatalytic performance[28, 29, 37].

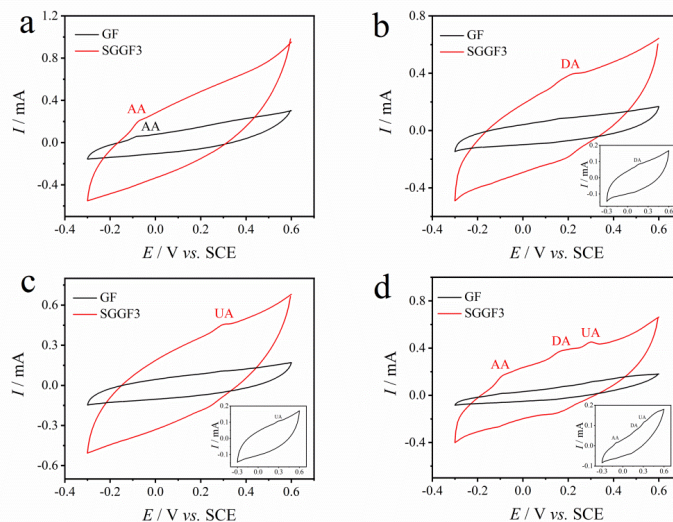


Figure 5. Electrochemical oxidation of (a) 3 mM AA, (b) 50 μ M DA, (c) 50 μ M UA, and (d) 3 mM AA, 50 μ M DA, 50 μ M UA on GF and SGGF electrodes, respectively, in 0.1 M phosphate buffer solution (PBS, pH=7), insets: magnified CV curves of GF.

3.4 Effect of scan rate and pH

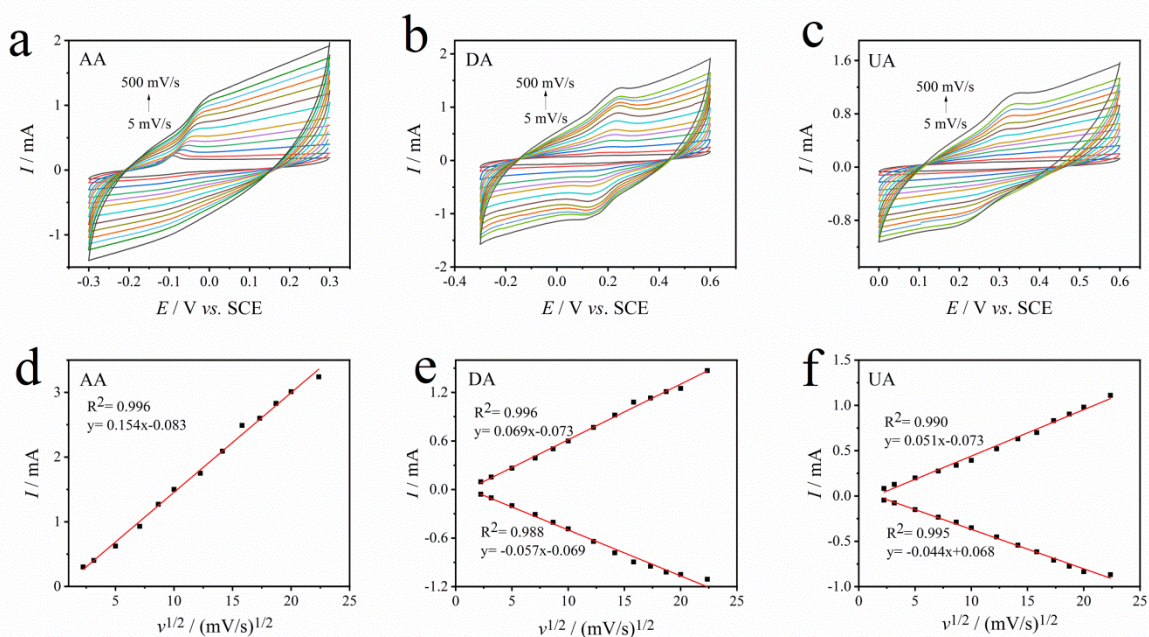


Figure 6. CV curves of (a) 5 mM AA, (b) 50 μ M DA, (c) 50 μ M UA at the SGGF3 electrode at various scan rate (5 – 500 $\text{mV}\cdot\text{s}^{-1}$). Plots of peak currents of (d) AA, (e) DA, and (f) UA versus the square root of the scan rate.

Figure 6 illustrates the voltammetric responses of AA, DA, and UA at the SGGF3 electrodes at varying scan rates. As the scan rate increased, the redox peak currents of the three species increased, whereas their redox peak potentials shifted to more positive and negative values. The redox peak currents are proportional to the square root of the scan rate, suggesting that their electrochemical reactions at the SGGF3 electrodes are under diffusion control in this scan rate range[3].

The influence of the pH of the solution on the electrochemical response was also studied. Figure 7a illustrates the differential pulse voltammetry (DPV) curves obtained in the solution with varying pH values. The oxidation peak potentials shifted to more negative values with increasing pH, indicating that proton transfer occurred in all reactions. The oxidation peak potential is linearly related to the solution pH, with slopes of 62, 57, and 36 mV/pH (Figure 7b). The slopes of UA and DA are close to the theoretical value of 59.2 mV/pH, indicating that the electrochemical oxidation reaction involves equal amounts of protons and electrons [41]. The lower slope of AA may be due to its oxidation being a $1e^-/2H^+$ process[3].

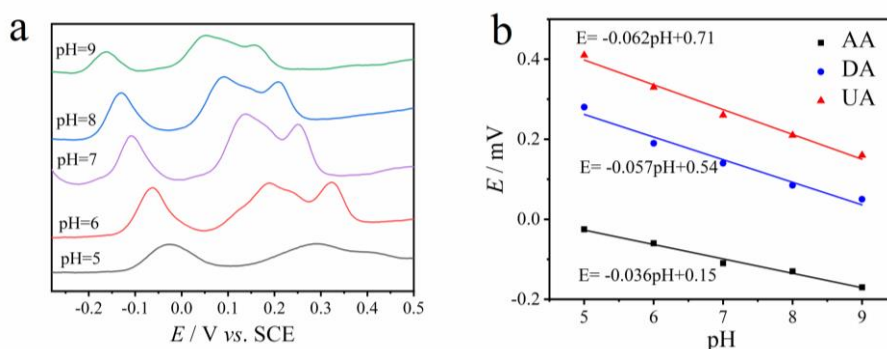


Figure 7. (a) DPV curves of SGGF3 in PBS with varying pH levels and (b) pH dependence of formal potential in DPV curves.

3.5 Electrochemical detection of AA, DA, and UA

AA, DA, and UA play a vital role in life activities and usually coexist; therefore, their individual and simultaneous determination are very significant. Individual determination was performed when the other two species coexisted; the results are shown in Figure 8. As shown in Figure 8a, the peak current of AA increased linearly with increasing AA concentration when 30 μ M DA and UA were present. The linear range for the determination of AA was 0.5 – 8 mM. The response of the SGGF3 electrode to DA and UA was similar to that of AA. The corresponding linear ranges were 1 – 30 μ M, and 5 – 100 μ M, respectively. The presence of the other two molecules did not interfere with the detection of the target molecule, indicating that the SGGF3 electrode exhibited excellent selectivity.

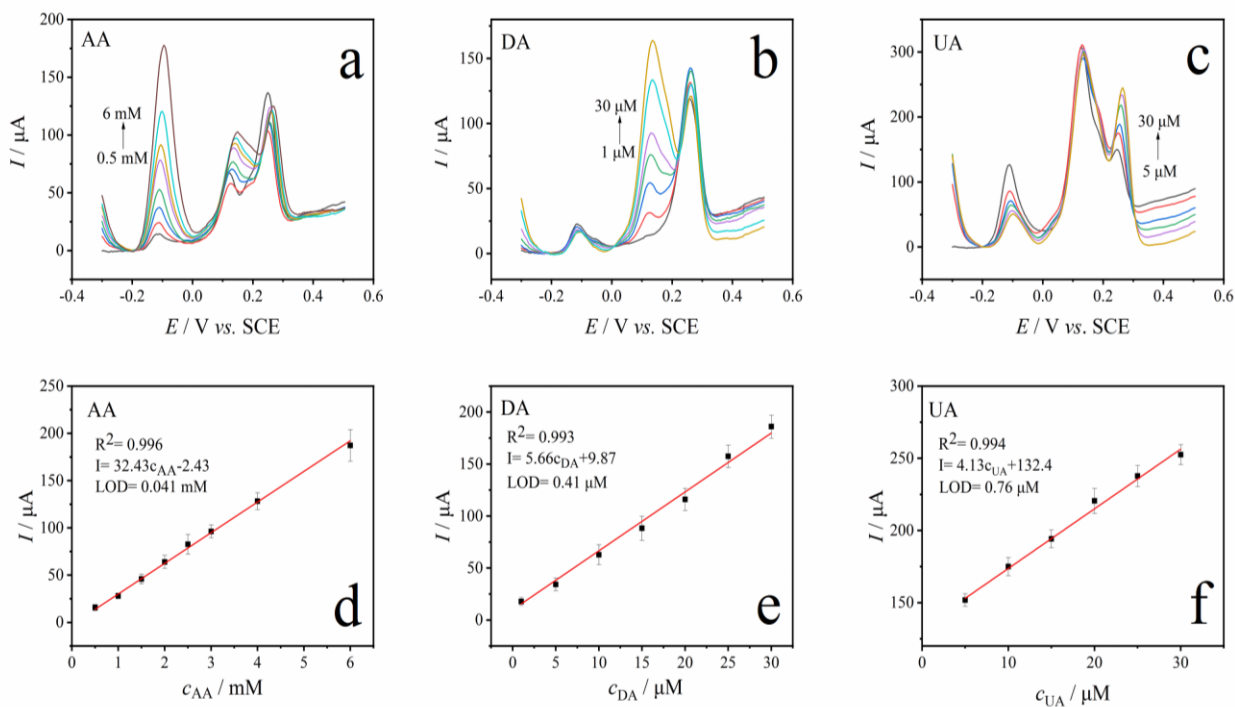


Figure 8. DPV curves of (a) 10 μM DA, UA, and AA in the range of 0.5 – 6 mM, (b) 1 mM AA, 30 μM UA, and DA in the range of 1 – 30 μM , (c) 1 mM AA, 50 μM DA, and UA in the range of 5 – 30 μM at SGGF3 electrodes in PBS (pH 7.0).

DPV tests were also performed in ternary mixtures of varying concentrations, as shown in Figure 9. The three separate peaks correspond to oxidation. The peak currents increased linearly with increasing concentrations in the ranges of 100 – 4000, 1 – 25, and 1 – 25 μM , with detection limits of 47, 0.12, 0.15 μM at S/N=3, respectively. Table 1 summarized the comparison of the analytical performance of SGGF3 and other electrodes[1, 2, 9, 33, 44]. The electrochemical performance of the SGGF3 electrode, which is attributed to its large specific surface area and S doping, is better than or comparable to that reported in previous study.

3.6 Reproducibility of SGGF3

Reproducibility is a crucial characteristic to evaluate the electrochemical performance of SGGF3. Five electrodes obtained under identical conditions were used to simultaneously detect AA, DA, and UA to assess reproducibility. The relative standard deviations of the current response of 0.5 mM AA, 1 μM DA, and 3 μM UA were estimated as 1.5, 2.2, and 3.3%, respectively, indicating excellent reproducibility of the prepared electrode.

4. CONCLUSIONS

A simple and economical electrochemical exfoliation method was used to modify GF with S-doped graphene. The SEM and XPS results demonstrated that doping occurred simultaneously during the exfoliation process. Owing to its large specific area and excellent conductivity, SGGF exhibited high electrocatalytic activity toward the oxidation of AA, DA, and UA, and it can be used as disposable electrodes in the detection AA, DA, and UA. The response of the SGGF3 electrodes to AA, DA, and UA indicated excellent sensitivity and reproducibility.

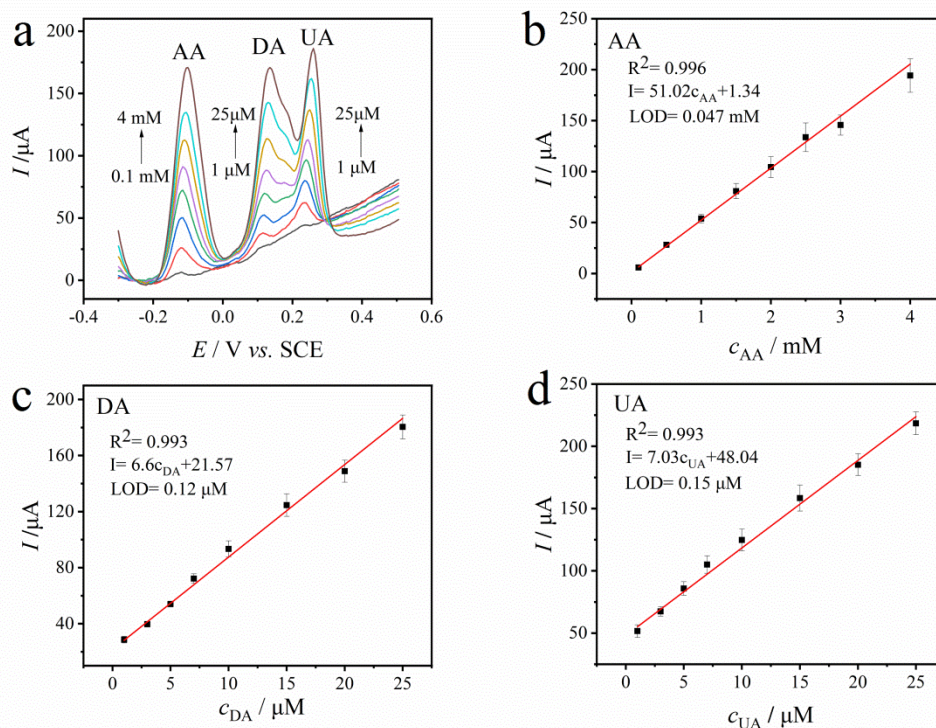


Figure 9. (a) DPV curves of varying concentrations of AA, DA, UA at the SGGF3 electrode, and the corresponding plots of peak currents vs. concentrations of (b)AA, (c) DA, (d)UA.

Table 1. Comparison of electroanalytical parameters of different electrodes for simultaneous determination of AA, DA, and UA

Electrode	Linear range/ μM			Detection limit/ μM			Ref.
	AA	DA	UA	AA	DA	UA	
MNC/GCE	1-700	0.001-30	0.01-800	0.01	0.001	0.001	[1]
GNSs/CC	20-1,000	0.5-20	0.5-20	0.31	0.01	0.03	[2]
RGO-CNT/ITO	10-200	0.2-8.0	0.2-16.0	5.31	0.04	0.17	[9]
3D NHPC	1.0-120.0	0.05-14.5	2.0-30.0	0.1	0.020	0.14	[33]
N-PCNPs	80-2000	0.5-30	4-50	0.7	0.011	0.02	[44]
SGGF	100-4000	1-25	1-25	47	0.12	0.15	This work

ACKNOWLEDGMENTS

This work was financially supported by Fundamental Research Funds for the Central Universities, China (N170504022).

References

1. A.Joshi, W. Schuhmann, T. C. Nagaiah, *Sensor Actuat B*, 230 (2016) 544.
2. S. Meng, Y. Liu, L. Wang, X. Ji, Y. Chen, T. Zheng, J. Yu, H. Feng, *Front Bioeng Biotechnol*, 9 (2021) 726071.
3. P. Kanyong, S. Rawlinson, J. Davis, *Chemosensors*, 4 (2016)25.
4. K.P. Aryal, H.K. Jeong, *Chem Phys Lett*, 768 (2021)138405.
5. D. Li, M. Liu, Y. Zhan, Q. Su, Y. Zhang, D. Zhang, *Microchim Acta*, 187 (2020) 94.
6. L. Zhao, H. Li, S. Gao, M. Li, S. Xu, C. Li, W. Guo, C. Qu, B. Yang, *Electrochim Acta*, 168 (2015) 191.
7. L. Zhang, J. Khungwa, Y. Liu, L. Li, X. Wang, S. Wang, *J Electrochem Soc*, 166 (2019) H351.
8. H. Wang, F. Ren, C. Wang, B. Yang, D. Bin, K. Zhang, Y. Du, *RSC Advances*, 4 (2014) 26895.
9. Y. Zhang, Y. Ji, Z. Wang, S. Liu, T. Zhang, *RSC Advances*, 5 (2015) 106307.
10. P. Shi, Y. Wang, X. Liang, Y. Sun, S. Cheng, C. Chen, H. Xiang, *ACS Sustain Chem Eng*, 6 (2018) 9661.
11. D. He, A.J. Marsden, Z. Li, R. Zhao, W. Xue, M.A. Bissett, *Electrochim Acta*, 299 (2019) 645.
12. J.M. Munuera, J.I. Paredes, M. Enterria, A. Pagan, S. Villar-Rodil, M.F.R. Pereira, J.I. Martins, J.L. Figueiredo, J.L. Cenis, A. Martinez-Alonso, J.M.D. Tascon, *ACS Appl Mater Interfaces*, 9 (2017) 24085.
13. Y.Z.N. Htwe, W.S. Chow, Y. Suda, A.A. Thant, M. Mariatti, *Appl Surf Sci*, 469 (2019) 951.
14. M.E.A. Ali, *Colloid Surface A*, 570 (2019) 107.
15. N. Liu, F. Luo, H. Wu, Y. Liu, C. Zhang, J. Chen, *Adv Funct Mater*, 18 (2008) 1518.
16. J. Lu, J.-x. Yang, J. Wang, A. Lim, S. Wang, K.P. Loh, *ACS Nano*, 3 (2009) 2367.
17. C.-Y. Su, A.-Y. Lu, Y. Xu, F.-R. Chen, A.N. Khlobystov, L.-J. Li, *ACS Nano*, 5 (2011) 2332.
18. J. Liu, C.K. Poh, D. Zhan, L. Lai, S.H. Lim, L. Wang, X. Liu, N. Gopal Sahoo, C. Li, Z. Shen, J. Lin, *Nano Energy*, 2 (2013) 377.
19. K. Parvez, Z.S. Wu, R. Li, X. Liu, R. Graf, X. Feng, K. Mullen, *J Am Chem Soc*, 136 (2014) 6083.
20. F. Sharif, A.S. Zeraati, P. Ganjeh-Anzabi, N. Yasri, M. Perez-Page, S.M. Holmes, U. Sundararaj, M. Trifkovic, E.P.L. Roberts, *Carbon*, 157 (2020) 681.
21. P.C. Shi, J.P. Guo, X. Liang, S. Cheng, H. Zheng, Y. Wang, C.H. Chen, H.F. Xiang, *Carbon*, 126 (2018) 507.
22. Y.L. Zhong, T.M. Swager, *J Am Chem Soc*, 134 (2012) 17896.
23. J. Wang, K.K. Manga, Q. Bao, K.P. Loh, *J Am Chem Soc*, 133 (2011) 8888.
24. Y. Yang, W. Shi, R. Zhang, C. Luan, Q. Zeng, C. Wang, S. Li, Z. Huang, H. Liao, X. Ji, *Electrochim Acta*, 204 (2016) 100.
25. M. Mooste, E. Kibena-Pöldsepp, B.D. Ossoonon, D. Bélanger, K. Tammeveski, *Electrochim Acta*, 267 (2018) 246.
26. D. Chen, F. Wang, Y. Li, W.W. Wang, T.X. Huang, J.F. Li, K.S. Novoselov, Z.Q. Tian, D. Zhan, *Chem Commun*, 55 (2019) 3379.
27. Y. Tian, Y. Liu, W. Wang, X. Zhang, W. Peng, *J Nanopart Res*, 17 (2015)193.
28. Y. Tian, Y. Ma, H. Liu, X. Zhang, W. Peng, *J Electroanal Chem*, 742 (2015) 8.
29. M. Li, C. Liu, H. Zhao, H. An, H. Cao, Y. Zhang, Z. Fan, *Carbon*, 86 (2015) 197.
30. H.L. Poh, P. Simek, Z. Sofer, M. Pumera, *ACS Nano*, 7 (2013) 5262.
31. N. Parveen, M.O. Ansari, S.A. Ansari, M.H. Cho, *J Mater Chem A*, 4 (2016) 233.
32. F. Lou, M.E.M. Buan, N. Muthuswamy, J.C. Walmsley, M. Rønning, D. Chen, *J Mater Chem A*, 4 (2016) 1233.
33. A. Nsabimana, J. Lai, S. Li, P. Hui, Z. Liu, G. Xu, *Analyst*, 142 (2017) 478.
34. L. Chao, Y. Qin, Y. Liu, Y. Kong, F. Chu, *J. Solid State Electrochem*, 21 (2016) 1287.
35. F. Liu, F. Niu, T. Chen, J. Han, Z. Liu, W. Yang, Y. Xu, J. Liu, *Carbon*, 134 (2018) 316.

36. W.-S. Jeon, C.H. Kim, J.-H. Wee, J.H. Kim, Y.A. Kim, C.-M. Yang, *Appl Surf Sci*, 558 (2021) 149867.
37. F. Shahzad, S.A. Zaidi, C.M. Koo, *Sensor Actuat B*, 241 (2017) 716.
38. H. Abe, K. Nozaki, S. Sokabe, A. Kumatani, T. Matsue, H. Yabu, *ACS Omega*, 5 (2020) 18391.
39. L. Cheng, Y. Hu, D. Qiao, Y. Zhu, H. Wang, Z. Jiao, *Electrochim Acta*, 259 (2018) 587.
40. D. Yuan, X. Yuan, S. Zhou, W. Zou, T. Zhou, *RSC Advances*, 2 (2012) 8157.
41. L. Yang, D. Liu, J. Huang, T. You, *Sensor Actuat B*, 193 (2014) 166.
42. S. Ding, M. Dai, X. Su, D. Guo, L. Bian, X. Liu, *J Electroanal Chem*, 915 (2022)116349.
43. X. Zhang, K.P. Wang, L.N. Zhang, Y.C. Zhang, L. Shen, *Anal Chim Acta*, 1036 (2018) 26.
44. P. Gai, H. Zhang, Y. Zhang, W. Liu, G. Zhu, X. Zhang, J. Chen, *J Mater Chem B*, 1 (2013) 2742

© 2022 The Authors. Published by ESG (www.electrochemsci.org). This article is an open access article distributed under the terms and conditions of the Creative Commons Attribution license (<http://creativecommons.org/licenses/by/4.0/>).